A Compressible Scaffold for Minimally Invasive Delivery Of Large Intact Neuronal Networks

Amélie Béduer, Thomas Braschler, Oliver Peric, Georg E. Fantner, Sébastien Mosser, Patrick C. Fraering, Sidi Benchérif, David J. Mooney, and Philippe Renaud*

Millimeter to centimeter-sized injectable neural scaffolds based on macroporous cryogels are presented. The polymer-scaffolds are made from alginate and carboxymethyl-cellulose by a novel simple one-pot cryosynthesis. They allow surgical sterility by means of autoclaving, and present native laminin as an attachment motive for neural adhesion and neurite development. They are designed to protect an extended, living neuronal network during compression to a small fraction of the original volume in order to enable minimally invasive delivery. The scaffolds behave as a mechanical meta-material: they are soft at the macroscopic scale, enabling injection through narrow-bore tubing and potentially good cellular scaffold integration in soft target tissues such as the brain. At the same time, the scaffold material has a high local Young modulus, allowing protection of the neuronal network during injection. Based on macroscopic and nanomechanical characterization, the generic geometrical and mechanical design rules are presented, enabling macroporous cellular scaffold injectability.

1. Introduction

It is a clinical observation that the adult human brain typically fails to repair large-scale tissue damage.[1] This contrasts with the observation that neurons are continuously generated in the subventricular zone and dentate gyrus,[2,3] and it is indeed the hope and aim of cell-based therapies to extend the brain's regeneration capacity to large-scale lesions. A major limitation on the path to successful neural tissue engineering and deep brain transplantation is the development of minimally invasive surgical techniques and scaffolds. Indeed, the surgical procedures involved in implanting complex and large solid grafts into the brain are very invasive and can easily lead to further tissue damage rather than the desired reconstruction outcome.[4] A number of minimally invasive delivery methods have been proposed, allowing to apply in situ gelling formulations, microparticulate scaffold suspensions, partially dissociated tissue, or neural stem cell suspensions through narrow-bore needles.[5–15] Unfortunately, without the guidance of a large-scale organized scaffold, the cells typically build chaotic structures rather than repairing the native tissue architecture as desired.[14] As a result, the associated functional recovery is never complete and data from successful human clinical studies are extremely scarce.[15] We propose here to address this current major bottleneck of neural tissue engineering by the use of a smart cellular scaffold system, which is highly and reversibly compressible, allowing for minimally invasive implantation of large, potentially preorganized constructs. To achieve this goal, several requirements must be met: The scaffold material must be highly compressible, such that mL-scale volumes can be delivered through narrow-bore tubing or needles, yet it should recover its original shape, volume and organization after the injection process. It should protect differentiated neurons with their extended neurites during the compression associated with the delivery process, but nevertheless behave as a globally soft material to minimize glial scarring reactions in the brain.[16] For the long-term culture necessary to develop differentiated neuronal networks, and in light of potential clinical translation, the scaffolds need to be reliably sterilized, preferentially by autoclaving. Last but not least, it is desirable to be able to provide native extracellular matrix (ECM) proteins to guide cell adhesion and differentiation. Macroporous scaffolds with shape memory amenable to injection through narrow-bore tubing can be fabricated by different techniques, such as emulsion polymerization, lyophilization, and cryogelation.[17–19] We base our scaffolds on the process of cryogelation, involving polymerization of a hydrogel precursor at subzero temperature, since this has been observed to produce particularly robust gels, and since the possibility of neuronal tissue engineering with cryogels has been reported.[19–21] We provide a novel cryogel fabrication paradigm, consisting of a

Dr. A. Béduer, Dr. T. Braschler, Prof. P. Renaud
STI-IMT-LMIS4, Station 17, EPFL
1015, Lausanne, Switzerland
E-mail: amelie.beduer@epfl.ch
Dr. T. Braschler, Dr. S. Benchérif, Prof. D. J. Mooney
School of Engineering and Applied Sciences
Harvard University,
02138, Cambridge, MA, USA
O. Peric, Prof. G. E. Fantner
STI-IBI-LBNI, Station 17, EPFL
1015, Lausanne, Switzerland
S. Mosser, Prof. P. C. Fraering
SV-BMI-CMSN, Station 15, EPFL
1015, Lausanne, Switzerland

DOI: 10.1002/adhm.201400250

simple one-pot carbodiimide-based cryosynthesis, and a coating method for native cell-adhesive proteins applicable after autoclave sterilization of the scaffolds. The newly developed protocol is the first to simultaneously address the requirement for autoclave sterilization, native ECM protein presentation, and scaffold injectability; at the same time, it avoids tedious precursor synthesis. It provides mL-scale scaffolds that can be injected through 1 mm needles while indeed protecting a live-extended neural network at cell densities approaching the one of native cortical gray matter. We also investigate the precise mechanical and geometrical properties providing for injectability and cell protection, by means of a novel atomic force microscopy (AFM) sample preparation technique and mechanical testing of the scaffolds. The shape-memory properties, finally, will allow adapting exactly the scaffold shape and volume, as well as cell density and neural growth to the tissue to be reconstructed, before in vivo injection. The system is therefore an ideal candidate for personalized tissue engineering.

2. Results

To prepare macroporous scaffolds suitable for 3D cell culture, we used a cryogelation process, which consists in hydrogel polymerization at subzero temperatures, using ice crystal formation to define the pore space. Hydrogels presented in this work consisted in sodium alginate and carboxymethylcellulose (CMC), selected for their known biocompatibility and potentially favorable effects on neurons in culture.[22–25] We initiate the polymerization via carbodiimide activation of the carboxylic acid residues on the carbohydrate moieties of the gel prepolymers, followed by amide bond formation with adipic dihydrazide, which results in the covalent crosslinking of the gels (details about the process are available in Supporting Information 1). Carrying out this process at subzero temperature allows creating macroporous hydrogels, referred to as cryogels, characterized by large interconnected pores, as schematized in **Figure 1**A. These scaffolds are sterilized by autoclave, coated with appropriate cell-adhesive molecules (poly-L-ornithine, PLO, and laminin), and finally seeded with neuronal cells. The cell-laden cryogels can be partially dehydrated, reducing the scaffold size, and allowing for injection of the cellular scaffold through a syringe needle, as shown in Figure 1A. After injection, cellular scaffolds retrieve their initial size and shape, by uptake of liquid injected along with the cryogel. Cell integrity and morphology are preserved throughout the injection process. Figure 1B presents scanning electron microscope (SEM) images showing the microscopic architecture of the cryogel scaffolds, made either from alginate or CMC. The cryogelation process resulted in highly porous structures for both polymers. The pore

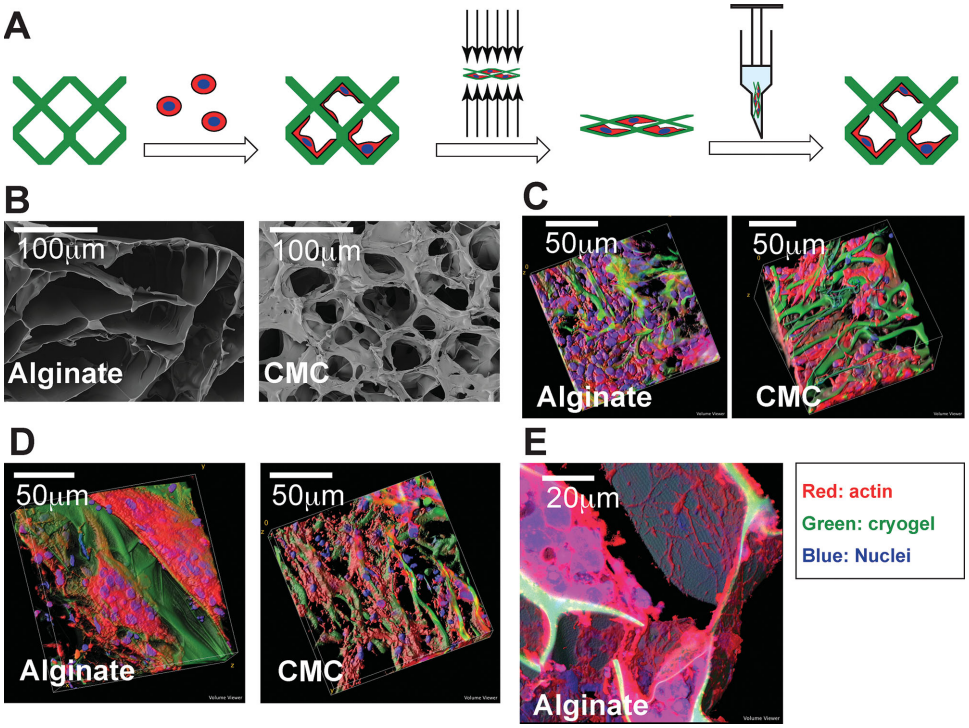

Figure 1. Structure, neuronal cell adhesion, and injection principle for macroporous alginate and carboxymethyl-cellulose (CMC) cryogels. A) Scaffold-protected injection of adherent cells: The cells are seeded on a macroporous cryogel scaffold coated with suitable adhesion motifs (poly-L-ornithine and laminin), and allowed to adhere and spread. The scaffold is then partially dehydrated, losing up to 90% of its volume without cell damage, and can be passed through an injection device such as a syringe before swelling back to its original volume. Cell integrity is protected throughout the process due to the particular mechanical and structural properties of the cryogels. B) Structure of alginate (3%) and CMC (1%) cryogels by scanning electron microscopy. C,D) Confocal micrographs of the human neuronal cell line SHSY-5Y (Figure 1C) and primary mouse cortical neurons (Figure 1D) on alginate and CMC cryogels. E) Closer view of a mouse primary neuron culture on a cryogel, showing the extensive neurite network visible on areas not covered by the cell bodies. For Figure 1C–E, the nuclei are blue (DAPI), the gel is labeled green (aminofluorescein, incorporated covalently), and the actin cytoskeleton is labeled red (rhodamine-phalloidin); all gels were coated with PLO/laminin.

Adv. Healthcare Mater. **2014**,
DOI: 10.1002/adhm.201400250

dimensions are comprised between 20 and 500 µm and depend on the exact cryogelation process parameters (details about pore volumes are given below). Cryogel formation using alginate as a starting material allowed obtaining 3D scaffolds with relatively thin walls (ca. 1–5 µm). They were somewhat thicker in the case of CMC-scaffolds (Figure 1B). After coating with PLO and laminin, the 3D scaffolds were seeded with neuronal cells (human neuroblastoma neuronal cell line SH-SY5Y or primary cortical mouse neurons). Seeding was carried out by first partially dehydrating cryogels (by pressing them against a sterile gauze) and rehydrating them with the cellular suspension. At the initial time of 3D plating, the dissociated neural cells had a spherical morphology, without visible neurites. Over time in culture, there was considerable process outgrowth resulting in the formation of 3D, interconnected neural networks. After 7 d of culture, cellular scaffolds were fixed and observed by confocal microscopy. Figure 1C,D present 3D confocal images of the resulting cellular scaffolds for the human neural cell line SH-SY5Y (1C) and primary cortical mouse neurons (1D). The analysis demonstrates a complex and dense cellular 3D architecture for both the human cell line and the mouse primary cortical neurons, for both alginate and CMC-based cryogels, with an approximately homogeneous cell density throughout the 1 mm thick scaffolds. In addition, the mouse primary neurons also presented a widespread and dense neural network, as exemplified in the zoomed view given in Figure 1E. Thus, the 3D cryogels developed here allow to obtain high cell density 3D cellular scaffolds on the millimeter size scale when coated with appropriate cell-adhesive motives. The process is versatile with respect to the choice of hydrogel and cell types.

In order to further characterize the interaction between cells and cryogel scaffolds, in particular regarding cell adherence, spreading and development, we further investigated the role of scaffold coating, mean pore volume, and polymer concentration. To do so, we quantified cell densities obtained on the scaffolds after 7 d of culture of the human neuronal cell line SH-SY5Y on different cryogel and control substrates, distinguishing "round cells" exhibiting rounded cell bodies without visible neurites, from "spread cells" exhibiting at least one sprouting neurite.

Figure 2A shows how different combinations PLO, a synthetic positively charged polyelectrolyte, and laminin, an ECM protein known to favor neurite development, affect the cell density and morphology on the cryogel scaffolds. Applying either PLO or laminin alone provides a statistically significant increase in overall cell adhesion (the total cell densities were $4.5 \pm 0.9 \times 10^6$cells mL^{-1} for PLO coating, $3.7 \pm 0.4 \times 10^6$ cells mL^{-1} for laminin coating versus $1.5 \pm 0.3 \times 10^6$ cells mL^{-1} for the control condition consisting in pristine alginate cryogels, $P < 0.001$ vs control in both cases), but the majority of the cells remained rounded. Only the combination of PLO followed by laminin allowed to obtain a high density of spread cells $43 \pm 6 \times 10^6$ cells mL^{-1} ($P < 0.001$ vs control) while keeping the round cell density low ($4.6 \pm 6 \times 10^6$ cells mL^{-1}, which is comparable to the round densities found for other coating conditions). Hence in the remainder of this report, the specific coating combination consisting in PLO, followed by laminin, was used for all cell culture experiments. Next, we investigated the role of scaffold mean pore volume on cell density and morphology. For this, we employed scaffolds with a mean pore volume ranging

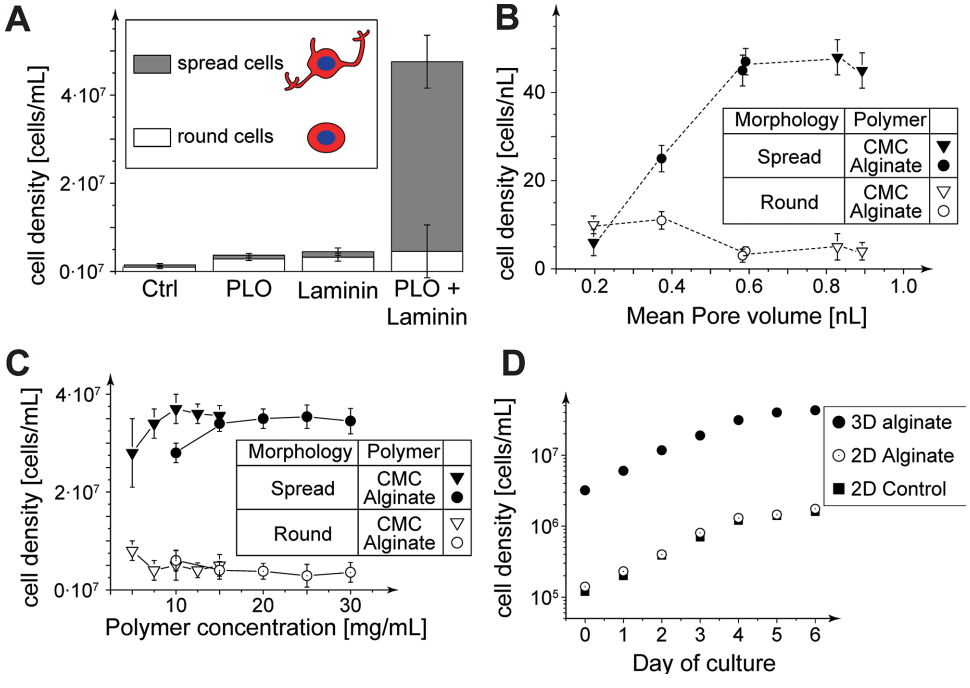

Figure 2. Parameters influencing cell adhesion and growth for the human neuronal cell line SH-SY5Y on the cryogels and 2D controls. A) The combination of PLO and laminin coating efficiently promotes cell attachment and spreading. B) Relation between pore volume and cell adhesion; the different pore volumes were obtained by varying the cryogelation substrate. C) Cell adhesion and spreading as a function of the original alginate or CMC concentration prior to cryogelation. D) Growth kinetics. With the exception of the specific conditions in Figure 2A, all cryogels as well as the 2D control substrates (Figure 2D) were coated with PLO/Laminin.

from 0.2 to 0.9 nL, obtained by modifying cryogel gelatin speed and polymer types . Figure 2B shows that the total cell density decreases significantly for pore volumes lower than 0.6 nL, with a concomitant relative increase in the ratio of round to spread cells. This indicates that the cryogel synthesis conditions should be chosen to achieve a mean pore volume of 0.6 nL or above. Figure 2C shows the effect of the polymer concentration in the initial reaction mixture on the cell density and morphology. We observe a slight decrease in cell density for the lowest polymer concentrations, most likely related to the difficulty encountered in manipulating the resulting very soft gels.

Next, we studied the effects of the cryogel scaffolds on cell duplication of the human neuronal cell line SH-SY5Y. Since both the scaffold material and the specific 3D configuration could potentially affect cell growth, we compared the growth curves obtained for 3D alginate cryogel scaffolds both to a control consisting of a plain coverslip, and a 2D alginate hydrogel (all PLO/Laminin coated). The results are summarized in Figure 2D. The sustainable cell density is higher on 3D scaffolds than on the 2D surfaces. The effect can clearly be ascribed to the 3D structure, since the mere presence of a 2D alginate substrate does not influence the sustainable cell density compared to the plain glass control. The growth rates on the other hand are comparable forall three configurations. This indicates that although the 3D cryogel configuration permits to achieve higher final cell densities, it has no influence on the replication rate per se. We obtained similar results for 2D and 3D CMC gels (data not shown).

The purpose of the cryogel scaffolds developed here is specifically to enable injection of preformed neural engineered tissue through narrow-bore tubing such as syringe needles. It is therefore of primary interest to analyze survival once cellular constructs have been injected through a syringe needle. For doing this, we quantified cell survival using the trypan blue test at 7 d post-seeding, for both the human neuronal cell line SH-SY5Y and mouse primary cortical neurons. We then performed syringe injections through a 16G needle (1 mm inner diameter), and quantified the cell viability again at 24 h and 48 h post-injection (the tests are performed on different samples to avoid artifacts due to trypan blue toxicity). Survival results obtained for human neural cell line and for primary mouse neurons are, respectively, presented in **Figure 3**A,B. Control conditions consisted in 2D surfaces made of alginate and CMC and also in plain glass coverslips. Viabilities for control conditions were quantified at the same time points with respect to the beginning of the culture as for the cryogel conditions but without the injection step.

Figure 3A indicates that cell survival scores did not decrease significantly following the cellular scaffold injection step for the SH-SY5Y cell line ($P = 0.86$ for alginate scaffolds 48 h after injection, $P = 0.92$ for CMC scaffolds 48 h after injection). Likewise, Figure 3B indicates that the injection step does not affect the viability of the mouse primary neurons on the 3D scaffolds, neither for the alginate nor for the CMC cryogels ($P = 0.90$ for alginate scaffolds 48 h after injection, $P = 0.86$ for CMC scaffolds 48 h after injection). This means that the cryogel scaffolds are able to protect not only the human cell line SH-SY5Y during the injection step, but also the more delicate primary neurons with their extended neurites. Figure 3A also indicates that the SH-SY5Y cells show very high and comparable survival rates regardless of the substrate (Alginate and CMC 3D scaffolds, 2D polymer substrates and glass coverslip control). In contrast, for the mouse primary cortical neurons, survival is significantly better on the 3D scaffolds than on the 2D controls (for example, cell survival on the 3D alginate scaffolds was 82 ± 8% compared to only 57 ± 7% on 2D alginate surfaces, $P < 0.001$). Indeed,

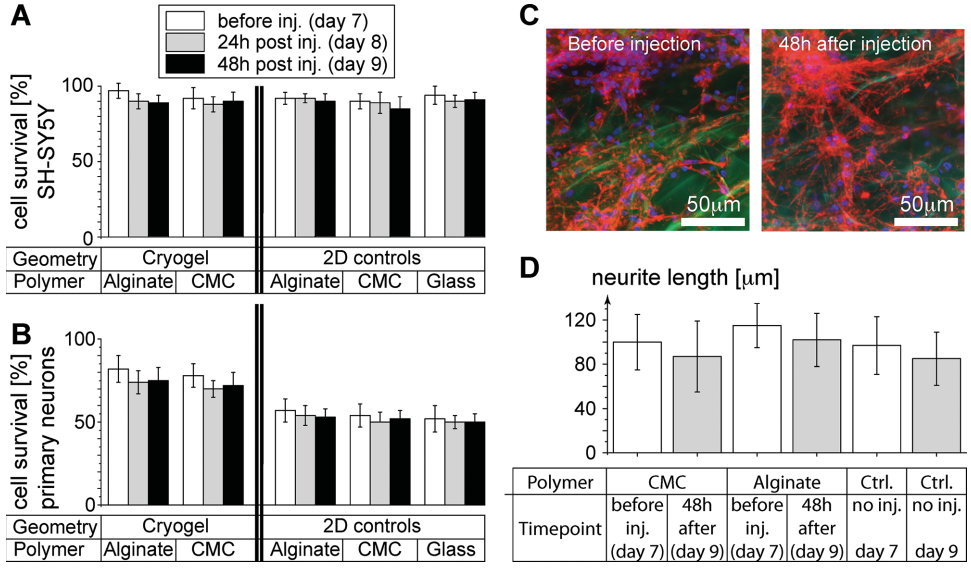

Figure 3. Cell survival and integrity during scaffold injection. A) Quantification of cell viability for the neuronal cell line SH-SY5Y before, 24 and 48 h after injection through a syringe. B) Quantification of cell viability for mouse primary neurons before, 24 and 48 h after injection through a syringe. The viabilities for the 2D controls in Figure 3A,B are taken at the same time points, but without the injection procedure. C) Representative images of mouse primary neurons on a cryogel before and 48 h after injection. Actin is labeled by means of rhodamine-phalloidin. D) Average neurite length extracted from images before and 48 h after injection. The cryogels used are synthesized in glass molds; both the cryogels and the 2D controls were PLO/Laminin coated.

DOI: 10.1002/adhm.201400250

the cell density obtained on 2D surfaces correspond to a high degree of confluence, which is apparently not very favorable for the survival of these primary cells under our culture conditions. In the 3D configuration, the resulting volumetric density is reduced, potentially explaining the better survival scores.

To assess the long-term outcome of CMC and alginate 3D scaffolds seeded with primary neural cells (40×10^6 cells mL^{-1}) were also maintained in culture during 21 d, with half-media change twice weekly from 7 d on. The survival scores on the cryogels remained comparable to the ones obtained for the 7-d culture: 87 ± 4% for alginate cryogels and 84 ± 6% for CMC cryogels.

Beyond cell survival, we also require the scaffolds to protect cell morphology during the scaffold injection step. Indeed, primary neurons develop dense neurite networks on the scaffolds, typically connecting clusters of neurons together; breakage of these networks must be avoided. Figure 3C presents z-projections of confocal images (observation thickness: 50 µm), before and 48 h post-injection, indicating qualitatively that no major damage to the neural network occurs. To quantitatively assess the neurite network before and 48 h after scaffold injection through a 1-mm syringe needle, we measured neurite mean lengths before and after the injection step for both type of cellular scaffolds (primary neurons grown on alginate and CMC cryogels) (Figure 3D). We observe that the injection step has no significant influence on neurite length ($P = 0.94$ for alginate scaffolds, $P = 0.95$ for CMC scaffolds). Furthermore, neurite lengths on 3D cryogels are comparable to those measured for neurons cultured on glass coverslips (control condition). Likewise, we measured the neurite length at 24 h and 7 d post-injection, and also found no significant difference to the respective controls. The successful protection of both cell viability and differentiated morphology despite the extensive volumetric compression of the scaffolds during syringe injection is a key result of the present study, underpinning the great potential of the 3D cellular injectable cryogels for neural tissue engineering and transplantation strategies.

In order to explain the observed neural protection during the compression associated with syringe injection, we characterized the mechanical properties of the cryogels both experimentally and theoretically. The characteristic highly porous structure of the cryogels (Figure 1B) suggests that they should behave as mechanical meta-materials,[26,27] with potentially very large differences between a locally stiff, cell-protective environment, and a low apparent macroscopic bulk stiffness, enabling extensive scaffold compression and ultimately syringe injection. Indeed, adapting a model from foam mechanics,[26,28] we obtain a simple relation between the apparent macroscopic stiffness, described by the bulk modulus B_{ulk} and the local stiffness of the cryogel wall material, described by the Young modulus E_{wall}. The development is given in Supporting Information 4, and yields (Equation S21, Supporting Information):

$$E_{bulk} = 2 * E_{wall} * \Phi^3 * F_{struct} \quad (1)$$

where Φ is the volume fraction occupied by the scaffold walls, and F_{struct} is a dimension-less structural factor, on the order of unity, and depending on the polymer-type. Equation 1 outlines the crucial importance of the wall volume fraction: with a wall volume fraction Φ in the range of 1%–10%, one may expect the cryogels to be 3 to 6 orders of magnitude softer globally than locally.

Atomic force microscopy has recently been identified as a useful tool to evaluate the local stiffness of cryogels.[27] Using this technique in conjunction with a specifically developed sample preparation method, we evaluated the wall Young modulus E_{wall} in an aqueous environment on covalently immobilized cryogel fragments on a glass coverslide (experimental details are given in Supporting Information 2). **Figure 4**A shows the topography of the immobilized cryogel fragments, whereas Figure 4B,C show close-up views of a fiber-shaped fragment along with the local Young modulus. The cryogel fragments appear as elevated areas on the topography image (Figure 4A,B), and as soft areas on the comparatively hard glass substrate in the Young modulus image (Figure 4C). Figure 4D shows the average Young modulus of the cryogel fragments as a function of the polymer type (alginate or CMC) and initial concentration used to synthesize the cryogels. While we find the alginate cryogels to be locally stiffer than the CMC cryogels (E_{wall} = 117 vs 4.2 MPa, **Table 1**), we also find the local stiffness to be independent of the initial polymer concentration ($P = 0.52$ for the alginate gels, $P = 0.39$ for the CMC gels).

Next, we determined the wall volume fraction Φ by weighing the cryogels in the fully hydrated state, and after forceful dehydration. The result is shown in Figure 4E. To a first approximation, we can consider the wall volume fraction to be proportional to the initial polymer concentration. This confirms that during the cryosynthesis, an approximately constant final polymer concentration is reached within the cryogel wall,[32] explaining the approximately constant Young modulus for each cryogel type (alginate and CMC, Figure 4D). Further, from the slope of the regression lines in Figure 4E, we can estimate the final polymer concentration in the scaffold walls for each of the two cryogel types. The results are given in Table 1. They indicate that while very high local polymer concentrations are reached indeed, the walls should still be considered to be hydrogels, since they contain more than 70% water by weight.

Finally, we examined apparent bulk modulus of the cryogels by means of compression of macroscopic samples (disks of 4 mm diameter and 1 mm height) with a mechanical testing device (details are given in Supporting Information 3). The resultant macroscopic Young moduli E_{bulk} were found to be in the kPa range (Figure 4F) rather than the MPa range observed for the local Young moduli. Furthermore, Equation 1 quantitatively links the bulk moduli to the local Young moduli (linear fit in Figure 4F), and also allows to determine the structural strength factor F_{struct} for each of the two polymers (Table 1). It is noteworthy that the CMC cryogels, despite a lower local Young modulus, are macroscopically stiffer at a given polymer concentration than the corresponding alginate cryogels. This is in part due to a higher volume fraction, but mostly due to a higher structural constant F_{struct}. Finally, Equation 1 also quantitatively explains mechanical data on cryogels presented by others, previously explained only qualitatively (detailed discussion in Supporting Information 4).[27]

Given the strikingly different local and bulk elastic properties of the cryogel scaffolds, we next investigated how the presence of relatively hard cryogel walls can protect the soft cells during

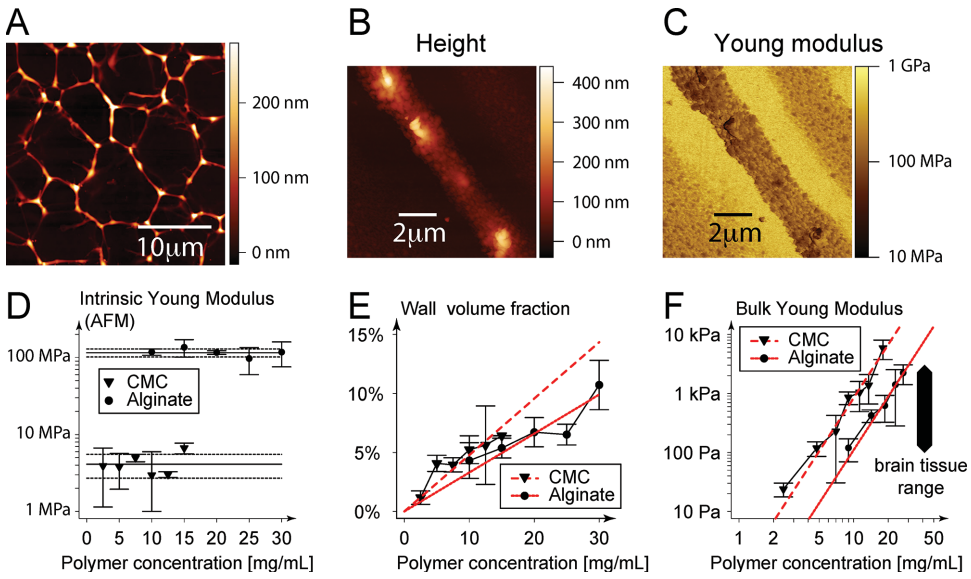

Figure 4. Microscopic and macroscopic mechanical properties of cryogels. A) Height image of CMC cryogel fibers immobilized on a glass substrate (1% initial CMC concentration) by atomic force microscopy (AFM). B) AFM Height image of a single alginate cryogel fiber (from a 1.5% initial alginate cryogel). C) AFM Young modulus map corresponding to Figure 4B, as determined by the quantitativenanomechanicalmapping in PeakForce Mode (PeakForce QNM). D) Intrinsic Young moduli of cryogel fibers from alginate and CMC cryogels with different initial polymer concentration, measured by AFM. E) Fraction of the volume occupied by the cryogel walls as a function of the initial polymer concentration. F) Apparent bulk Young moduli as a function of initial alginate, respectively, CMC concentration, determined by mechanical testing of macroscopic cryogel samples, along with best fit theoretical lines relating intrinsic modulus, wall fraction and apparent bulk modulus. The range of Young moduli for brain tissue is taken from literature.[29–31]

Table 1 Estimated intrinsic local and apparent bulk mechanical parameters of the alginate and CMC cryogels. The errors for the intrinsic Young modulus are the standard deviations of the means; the errors for the polymer concentration within the cryogel fibers are obtained from the linear regression (Figure 4E); the error on the structural factor results from the associated linear regression (Figure 4F) and propagated errors from the intrinsic Young modulus measurement as well as the estimation of the polymer concentration within the cryogel fibers.

Polymer	Intrinsic Young modulus [MPa] (Figure 4D)	Polymer concentration within the cryogel fibers [% w/w] (Figure 4E)	Structural factor F_{struct} (Figure 4F)
Alginate	117 ± 14	27.2 ± 1.9	0.013 ± 0.004
CMC	4.2 ± 1.4	19.4 ±1.5	0.92 ± 0.52

the compression process. For this, we used finite element modeling (FEM, carried out in the COMSOL software suite) of a simplified cryogel structure, comprising a simplified pair of adherent neurons with neurites (**Figure** 5A). As a control, we also simulate the same cell geometry, but embedded in a homogeneous gel without pores (Figure 5D). We chose the Young moduli of the different elements to reflect approximately the situation in a 1% CMC cryogel. According to Table 1, the local Young modulus should be 4.2 MPa; the wall volume fraction is about 4.3% (Figure 4E), so together with a structural factor of 0.92 (Table 1), one would expect an apparent global Young modulus on the order of 0.6 kPa for the cryogel (Equation 1). Hence, we used $E = 0.6$ kPa for the homogeneous control gel. The cells, including the neurites, are modeled with a Young modulus of 0.2 kPa, taken from literature.[33]

For the cryogel structure and the homogeneous control, we attempted to simulate the deformation and corresponding mechanical stresses using COMSOL for a uniaxial compression of 25% and 75%. We report the resulting von Mises stress, since this measure has been shown to be a good indicator of the probability of material failure under various load conditions. The cryogel structure easily admits 75% compression and beyond, the resulting von Mises stress distribution is shown in Figure 5B,C, respectively. On the contrary, the simulations for the homogeneous gel do not converge beyond 30% compression, enabling us to estimate the von Mises stress only for the 25% compression case (Figure 5E). The non-convergence for larger compression agrees with what would be observed if these experiments were carried out physically: while a cryogel would survive a 75% compression and beyond while maintaining mechanical integrity, a bulk gel would burst if compressed beyond some 20–30%.[19]

The distribution of the von Mises stress shows that in the case of the cryogel, the hydrogel absorbs almost all the elastic energy (Figure 5B,C), whereas in the bulk gel, the elastic energy transmitted to the gel respectively the cells is similar (Figure 5E). As a result, the cells are exposed to higher stresses in the bulk gel at similar compression (**Table 2**).

Taken together, these results indicate that accumulation of elastic energy by the cryogel structure, rather than transmission to the cells, offers the mechanical protection enabling high compression fractions while preserving neurons and extended neurites during the injection procedure. The high pore fraction, the small wall thickness, and the locally high Young modulus all contribute to this phenomenon (see Supporting Information 5 and discussion part for details).

In order to facilitate the use of the injectable cryogels scaffolds in different settings, we further investigated how different

Adv. Healthcare Mater. **2014**,
DOI: 10.1002/adhm.201400250

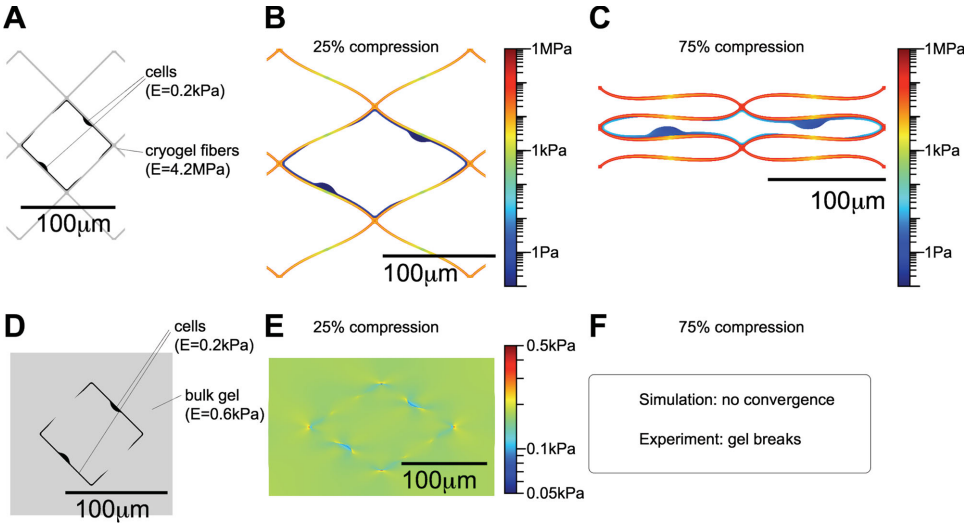

Figure 5. Finite element simulation. A) simplified structural model of the cryogel with a pair of adherent cells. B) Finite element simulation of a 25% compression of the cryogel. The deformation is imposed and corresponds to 25% of the height of the cryogel structure; the colors code for the von Mises stress, a known overall measure for material loading. C) Finite element simulation of a 75% compression of the cryogel structure. D) simplified structural model of a corresponding bulk gel with identical cell geometry and a bulk Young modulus corresponding to the apparent bulk modulus of the cryogel. E) Finite element simulation of a 25% compression of the bulk gel with cells, with imposed deformation. The colors again code for the von Mises stress, although it should be noted that the scales are different for Figure 5E as compared to Figure 5B,C. F) For 75% compression, the FEM simulation for the homogeneous control gel does not converge.

Table 2. Maximum von Mises stress sustained by the cells.

	25% Compression	75% Compression
Cryogel	15 Pa	46 Pa
Bulk gel	222 Pa	Not applicable (gel breaks)

synthesis parameters affect the final cryogel scaffold structure and performance. Results are presented in **Figure 6**. First, we compared three freezing strategies involving different substrates (Figure 6A): A first strategy consisted in pipetting the prepolymer solution onto a precooled Teflon plate (row "Teflon" in Figure 6A); a second strategy consisted in sandwiching the prepolymer solution between two glass cover slides by means of 1 mm high plastic spacers, and then placing the assembly on a preooled aluminum plate (row "Glass" in Figure 6A); the third strategy consisted in pipetting the prepolymer solution directly onto the precooked aluminum plate (row "aluminum" in Figure 6A). In each case, we assessed the linear pore dimensions and calculated the mean pore volume. We also calculated an anisotropy index, corresponding to the largest pore diameter divided by the smallest one on 2D sections. The smallest and most isotropic pores are observed for the "aluminum" scenario. This is expected, since aluminum has by far the highest thermal conductivity of the three substrates used,[34,35] and since it is well known that cryogels with smaller pores are generally obtained for the highest freezing rates due to the increased ice crystal nucleation rate.[36] Figure 6B summarizes the maximum volumes that we succeeded to inject through a 16G syringe needle without breakage, for gels of different composition (alginate or CMC, with and without PLO/Laminin coating) and pore volume. The maximum cryogel scaffold volume successfully injected was 3 mL, obtained with a coated CMC-cryogel, exhibiting the smallest pore size. Larger volumes have not been investigated. Contrary to Figure 6B where we injected cryogel scaffolds a single time, for Figure 6C, we injected a standard spherical cryogel scaffold of 100 µL through a 16G syringe needle (1 mm inner diameter), and quantified the number of times we could repeat the process before the cryogel would break into pieces. Since in practice, one would inject a cryogel only a single time, this gives a safety margin in terms of gel integrity. We find a relatively narrow optimum of prepolymer concentration for each polymer: 0.75% prepolymer concentration for the CMC cryogels and 2% prepolymer concentration for the alginate cryogels. In addition, we show that the PLO/Laminin coating reinforces the gel and makes it more robust against breakage. Figure 6D finally shows pore interconnectivity as assessed by the wicking test;[19] for CMC cryogels, we observe a drop in pore interconnectivity beyond 1% prepolymer concentration, while the alginate cryogels show high interconnectivity throughout the entire concentration range.

3. Discussion

In neural tissue engineering, the use of scaffolds serving as organized cell carriers is considered necessary due to the low cell survival and engraftment efficiency observed for cells transplanted in suspension.[37,38] The surgical procedures needed to place scaffolds of clinically relevant size are however associated with a high risk of further tissue damage.[6] To the best of our knowledge, there is still no solution able to simultaneously address large-size tissue reconstruction, potentially deep inside the brain, and to provide preorganized neural tissue constructs. Here, we present a novel type of highly compressible cryogel

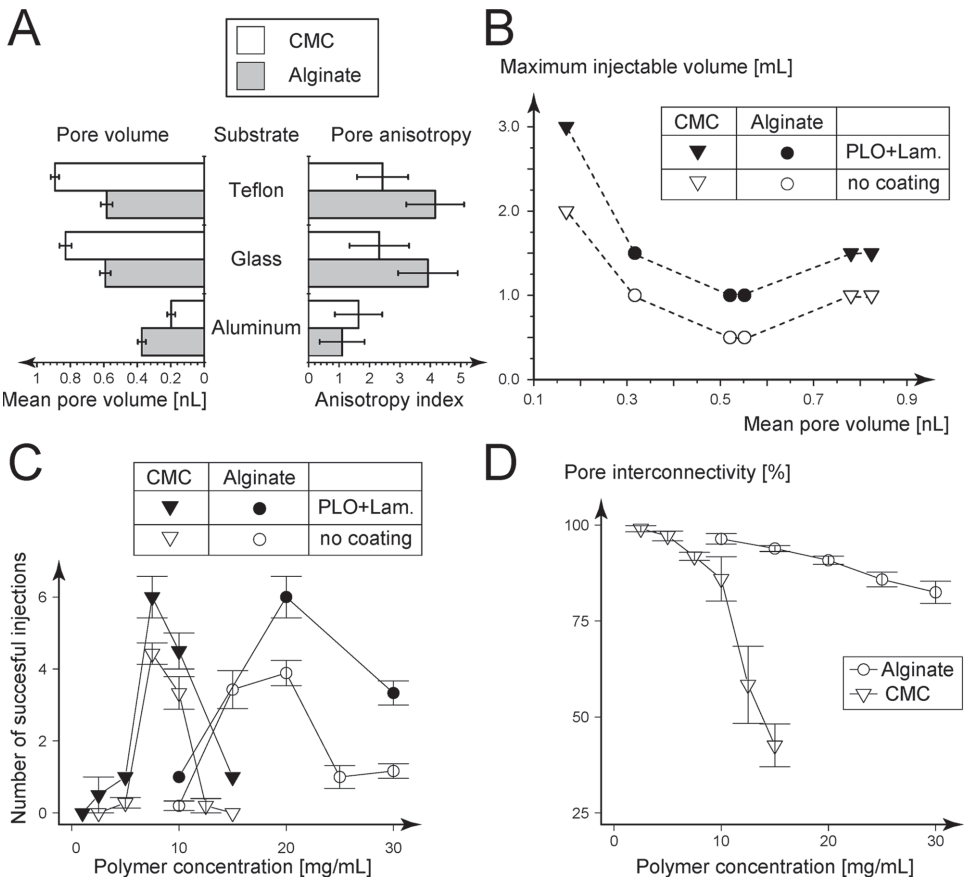

Figure 6. Control and optimization of the structural parameters and injectability of the cryogels. A) Cryogelation on different substrates affects pore size and pore anisotropy. B) Maximum injectable volumes (spherical gel geometry, injection through a 16G needle). C) Injectability as a function of the initial polymer concentration and the coating. Cryogelation performed on glass substrates. D) Pore interconnectivity as a function of the initial polymer concentration. Cryogelation performed on glass substrates. The errorbars indicate standard deviations of the mean.

scaffold, specifically adapted to minimally invasive delivery of differentiated neuronal networks by transient compression to about 10% of the initial volume. Based on a novel one-pot carbodiimide cryogel synthesis, the scaffolds advantageously combine desirable properties: They allow attachment, spreading and neurite formation by primary neurons due to the presentation of native laminin.[21] Their highly porous nature allows injection through narrow-bore tubing.[18,19] The scaffolds also present the advantage of reliable sterilization, of prime importance in light of potential clinical translation: By performing the deposition of the cell-adhesive coating only after cryogel synthesis, we are able to avoid microbiologically unsafe washing with ethanol solutions, which had to be employed with cryogel scaffolds having laminin or RGD peptides incorporated already during the synthesis step.[19,21,39] Further, the scaffolds extend the domain of volumes injectable through a 16-Gauge (1 mm) needle into the mL-range. Taken together, these properties enable the development of an extended neuronal network made from primary cells that can subsequently be highly compressed for minimally invasive delivery into the central nervous system. It is, to the best of our knowledge, the first demonstration of a compressible living neural network.

We find the success of cell seeding, attachment, and spreading on the cryogel scaffolds to be critically dependent on the prior coating of the cryogels with suitable cell adhesive motives (here, the combination of PLO and laminate, Figure 2A), confirming findings for neuronal culture on other substrates.[40] We also find a minimal pore volume of 0.6 nL to be required for optimal adhesion and spreading (Figure 2B), corresponding to a mean pore diameter of about 100 µm, in line with results reported for neural tissue engineering.[21] Additional important architectural parameters are the total pore fraction (Figure 4E: $1-\phi = 89\%$ for the 3% alginate cryogels, and >90% for all other compositions, in accordance with literature recommendations)[41] and also the fraction of the pore space interconnected[42] to the outside world (>80% for all scaffolds except the CMC 1.25% and 1.5%, Figure 6D) since only the accessible pores will be colonized. Provided suitable cell-adhesive coating, pore size, and interconnectivity, the cryogels support live cell densities up to 50×10^6 cells mL^{-1}, for both the human neuronal cell line SH-SY5Y (Figure 2) and mouse primary neurons (data not shown), for culture periods beyond 1 week. These cell densities approach the ones found in the mouse cortex (92×10^6 cells mL^{-1}), and exceed the live densities achievable with homogeneous gels by about one order of magnitude.[43,44] The 3D structure, with its high available surface area and high pore space for nutrient diffusion, rather than the specific material, is responsible for sustaining high viability at these high cell densities (Figure 3B).

Adv. Healthcare Mater. 2014,
DOI: 10.1002/adhm.201400250

Beyond attachment, the cryogel coating also provides cues for cell spreading (Figure 1E), and neurite extension by the mouse primary neurons (Figure 1E, Figure 3C,D). At the same time, neural cells also need to communicate with their peers.[45–47] In the cryogel scaffolds, we find that the neurites largely follow the gel walls, but are also able to bridge small gaps (Figure 1E). In addition, the somata of individual cells are found to adhere to the cryogel walls; but with higher cell density, organized multilayered structures are also formed (Figure 1E). This suggests an equilibrium between strong cell–matrix interaction and cell–cell interaction, which is considered suitable for tissue formation. Indeed, if the cell–matrix interaction is too strong, the cells will line the scaffold surface with minimal 3D organization and potentially loss of cell functionality;[46] if the cell–matrix interaction is too weak, the cells tend to adopt rounded morphology, and oftentimes undergo cell death due to lack of adhesion.[48]

In order to identify criteria to enable injection of the cellular scaffolds, we carried out bulk and nanomechanical characterization. By aligning the results obtained on the alginate and CMC cryogels, we are able to establish the following design rules for scaffold injectability (Supporting Information 5): minimal bulk Young modulus ($E_{bulk} \geq 0.1$ kPa) and minimal microscopic Young modulus ($E_{wall} \geq 100$ kPa) for appropriate manual handling, maximal wall volume fraction ($\Phi < 10\%$) for limiting local strain (Equation S29, Supporting Information), and high pore interconnectivity for enabling fluid evacuation. The protection of the cells during the injection process is due to the concentration of the elastic energy within the cryogel material (Figure 5). The nanomechanical analysis confirms the high local Young moduli necessary for this (Figure 4D, Table 1: E_{wall} = 117 MPa for alginate-based cryogels, respectively, 4.2 MPa for CMC-based cryogels). The high local Young modulus may also be advantageous in terms of neurite formation, since stiffer substrates have been linked to the formation of both more numerous and more highly branched neurites.[49]

The macroscopic compression analysis on the other hand confirms the low bulk stiffness (Figure 4F, 0.85 kPa for the 1% CMC vs 2.2 kPa for the 3% alginate cryogels used in the cell culture and live injection experiments), facilitating compression prior to injection with minimal force. In addition, the brain is a relatively soft organ, with elastic moduli reported in the 0.1–3 kPa range, depending on the region and measurement technique employed.[29–31] Since it has been reported that mismatch between the local stiffness and implanted devices may be linked to a strong adverse glial reaction,[16] it may be necessary to match the bulk stiffness of the scaffold to the local brain tissue Young modulus for in vivo experiments. Given the strong dependence of the bulk modulus on the initial polymer concentration (Figure 4F), it is straightforward to match to any desired Young modulus in the range reported for the brain; the necessary initial polymer concentration can indeed be calculated by Equation 1.

Finally, we demonstrate that cryogels with neurons exhibiting already substantial neurite extension can be compressed and syringe-injected, without damaging the cells (Figure 3). To the best of our knowledge, these scaffolds are the first to combine macroscopic size and injectability through a narrow-bore conduit for neuronal tissue engineering applications. The results demonstrate that suitably designed macroporous scaffolds allow to protect morphologically differentiated primary cells, going a fundamental step beyond the demonstration of injectability of cell suspensions or robust cell lines along with shape-memory scaffolds.[18,19] Given that cell density, neurite development and scaffold organization are preserved throughout the injection process, the scaffolds will allow to transfer in vivo not only the cells, but also their precise spatial organization.

4. Conclusions

We present a novel neural engineering scaffold that can be injected through a syringe needle, while conserving cell viability, morphology, and organization as well as scaffold integrity, even in the presence of differentiated neurites. The system is an answer to a major dilemma encountered in neural tissue engineering for the central nervous system: scaffolds should be preorganized and potentially large, but at the same time they should be delivered in a minimally invasive fashion to avoid further tissue damage. The scaffolds developed here are both: organized at a large size scale, and nevertheless injectable thanks to their compressibility. They open up an avenue of experiments and approaches hitherto thought impossible: spatial localization of adhesion motives and cells could be used to organize the scaffold into physiologically relevant regions, while chemical gradients could be used to guide long range connections before implantation. The features obtained could be quality-checked before implantation, and then minimally invasively delivered while maintaining shape, volume, viability, and neural network organization.

5. Experimental Section

Chemicals: The following chemicals were obtained from Sigma–Aldrich: Sodium alginate (catalog number A0682-100 G, molecular weight $\overline{M}_n$ = 110 kDa, $\overline{M}_w$ = 242 kDa, polydispersity 2.2 by gel permeation chromatography), sodium CMC (419338-100 G, 700 kDa according to the manufacturer's datasheet), *N*-(3-dimethylaminopropyl)-*N*'-ethylcarbodiimide hydrochloride EDC (E7750-25G), Morpholinoethanesulfonic acid MES hydrate (M2933-100G), adipic acid dihydrazide (AAD) (A0638-25G), aminofluorescein (07980 Fluka-1G), NaOH (S8045–500G), ethylene-diamine-tetraacetic acid EDTA (EDS), phosphate buffered saline (PBS) (P4417-50TAB), laminin (L-2020), paraformaldehyde,(158127-500 g) Triton X-100 (X100–100 mL), papain. Fetal bovine serum was obtained from PAA Laboratories, DMEM cell culture medium, penicillin streptomycin from GIBCO, neurobasal medium, and B27 from Invitrogen, and Glutamax from Life Technologies.

Cryogel Synthesis: Cryogels were synthesized based on established carbodiimide chemistry.[50] Details are given in Supporting Information 1. Briefly, either alginate or CMC is dissolved in deionized water (DI) to the desired concentration, and crosslinking initiated by means of addition of AAD and a small excess of the carbodiimide EDC. The reaction mixture is rapidly placed at –20 °C in a mold, resulting in ice crystal formation prior to completion of gel crosslinking; if not specified otherwise, cryogels were formed on molds made from glass coverslides and suitable spacers (Supporting Information 1). After 24 h, the cryogels are thawed, washed in DI, EDTA 10×10^{-3}M and PBS, and autoclaved in PBS; the space occupied by the ice crystals during the cryo-incubation now becomes pore space. If not specified otherwise, alginate cryogels were synthesized using the 3% composition as listed in Table S2 (Supporting Information 1), whereas CMC cryogels

were synthesized according to the 1% composition listed in Table S3 (Supporting Information 1). For visualization purposes, we also synthesized fluorescent cryogels by addition of aminofluorescein during the crosslinking reaction, since aminofluorescein will react with EDC-activated carboxylic acid groups under the same conditions as AAD (for details, see Supporting Information 1).[51]

SEM: Cryogel samples were lyophilized, gold coated and imaged using a Zeus's Merlin SEM operated at 5 keV and secondary electron detection.

Pore Fraction and Interconnectivity: The pore fraction and interconnectivity can be estimated from the weight loss under different dehydration conditions. The interconnected pore space is assessed by the wicking test, that is by the relative amount of water that can be withdrawn from a fully hydrated cryogel by means of a paper towel.[19] Similarly, the total pore space can be assessed by force-full compression (estimated mechanical pressure on the order of 1 MPa). The wall volume fraction, finally, is calculated as 1 minus the fraction occupied by the pore space.

Bulk Young Modulus: Bulk Young moduli were obtained by mechanical compression of cryogels with a defined disk geometry (typically, 4 mm diameter, 1 mm height). The measurements were performed on a TextureAnalyzer TA.XT plus (Stable Microsystems). Sample force–distance curves and the fitting procedure to obtain the Young moduli are given in Supporting Information 2.

Local Young Modulus by Atomic Force Microscopy: The local Young modulus of the cryogel fibers was determined by AFM imaging using the PeakForce Quantitative Nanomechanical Mapping (QNM) mode (Bruker, FastScan). To enable AFM imaging and Young modulus quantification, cryogel fibers with a height ranging from 50 nm to 1 µm were immobilized on an otherwise flat substrate. Supporting Information 3 provides the experimental details on the immobilization and imaging procedures; a comparison to Force–Volume imaging and COMSOL simulation of the hydrogel indentation process to evaluate the influence of the underlying substrate and the tip geometry are also provided.

Syringe Injection: For systematic injection tests, roughly spherical cryogels of 100 µL (ca. 6 mm in diameter) were prepared for various concentrations of alginate and CMC according to the protocol given above and detailed in Supporting Information 1. The finished cryogels were dehydrated by mechanical compression against a gauze, inserted into a syringe, and pushed through a syringe needle measuring 1 mm in inner diameter (16 Gauge). To investigate maximal injectable cryogels volumes, spherical cryogels of different volumes were fabricated and injected once through the same syringe needle. Injection was considered successful when the cryogels remained visually intact after the injection process.

Pore Volume and Anisotropy: Cryogels were cut into thin slices along two perpendicular directions while still frozen. After thawing, images were taken using a bright-field microscope (×10 objective), binarized, and the dimensions of at least 200 pores for each fabrication condition and cryogel composition were recorded using ImageJ software. The pore volume was estimated as the product of biggest, smallest, and mean pore diameter, whereas the pore anisotropy was calculated as the ratio between the biggest and the smallest pore dimension.

Cryogel Coating: Unless specified otherwise, autoclave-sterilized cryogels were coated prior to cell culture to allow the cells to adhere to the cryogel scaffolds. To do so, cryogel samples were first partially dehydrated by compressing them mechanically against a sterile gauze. A PLO (1 mg mL^{-1} diluted in sterile deionized water) droplet of 10 times the cryogel volume was then deposited on top of each cryogel and left for 1 h at 37 °C. The PLO droplet was then removed, and the cryogel samples rinsed with DI water. Finally, the cryogels were again partially dehydrated under sterile conditions, and laminin (1 µg mL^{-1} in sterile DI water) was added onto the cryogel samples (1× cryogel sample volume) and left for 4 h at 37 °C. Prior to initiation of cell culture, samples were rinsed with sterile DI water and compressed again immediately before cell seeding.

2D Control Substrates: 2D control samples for alginate and CMC substrates were fabricated on coverslips. To ensure permanent adhesion of the hydrogels to the glass slides, the coverslips are first coated with a molecular adhesion layer of alginate or CMC. The procedure coincides with the coverslide activation step used in the AFM sample preparation, given in Supporting Information 3. Once these molecular adhesion layers established, we deposited the bulk gel layers. To do so, we used the 1% recipe for the CMC and the 3% recipe for the alginate also used for the cryogel fabrication (Supporting Information 1), but rather than placing the reaction mixture at –20 °C, we dried a drop of the reaction mixture on the coverslides prior to completion of polymerization by using a stream of pressurized air. To ensure complete polymerization, we expose the dried slides to 170 °C dry heat for 20 min; to remove unreacted products, we sequentially washed them in NaOH 100×10^{-3}M, EDTA 10×10^{-3}M, and PBS, prior to 70% ethanol sterilization.

Neuronal Cell Line: The human neuroblastoma-derived cell line (SH-SY5Y) was grown in DMEM medium supplemented with 10% fetal bovine serum and 1% penicillin streptomycin in Petri dishes. Cells were subculture twice a week, and maintained at 37 °C and 5% CO_2. All reported experiments were performed using cells with less than 20 passages from purchase.

Primary Cortical Cells: All experimental procedures were carried out according to the Swiss federation rules for animal experiments. Mouse primary cortical neurons were prepared from embryonic day 17 Of1 fetal mouse brains. Cortices were digested in medium containing papain (20 U mL^{-1}) and dissociated by mechanical trituration. Cells were plated in neurobasal medium supplemented with 2% B27 and 2×10^{-3}M Glutamax. Unless otherwise specified, all substrates (cryogels, but also planar control substrates) were coated with PLO/Laminin as described above. All cells were kept in a humidified 5% CO_2 atmosphere at 37 °C.

Cryogel Seeding and Culture: SH-SY5Ycells or mouse primary cortical neurons were seeded onto cryogel and control substrates at a typical density of 4000 cells mm^{-3}. A droplet (volume equal to the cryogel volume) containing the cells is placed onto the partially dehydrated cryogel sample and incubated for 45–60 min. Cell culture medium (500 µL) was then added and cells were maintained at 37 °C, 5% CO_2. At experimental endpoints, the cellular scaffolds or control substrates were fixed with 4% paraformaldehyde for characterization. Cell distribution was homogeneous throughout the 1 mm thick scaffold. For culture periods beyond 7 d, half-media were changed twice weekly.

Analysis of Cell Morphology: To observe cells and quantify their morphology, cells were fixed with 4% buffered formaldehyde during 20 min. After PBS washes, actin cytoskeleton and cell nuclei were stained (permeabilization with Triton X-100 (0.3% in PBS), followed by phalloidin-Atto565 (Sigma–Aldrich) at a dilution of 1:200 and 4′-6-diamidine-2-phenyl indole (DAPI) used at 300×10^{-9}M). Fluorescence images were acquired using a confocal fluorescent microscope Zeiss LSM 700 with a –20× air objective or with a 40× oil objective. Images of at least 200 cells on four randomly chosen observation fields were captured and analyzed for each experimental condition and for each experiment. Experiments were repeated at least three times. Cell density was quantified as the number of cell nuclei in a given volume. SH-SY5Y cells were designated as "spread" when they developed at least one sprouting neurite from the soma measuring at least 15 µm in length, otherwise, they are considered "round." Based on confocal images, neurite length was measured using the plugin NeuronJ of ImageJ. For cell survival analysis, samples were rinsed with HEPES-buffered salt solution (HBS), and incubated in a trypan blue solution (0.4% in HBS) for 2 min at room temperature. The samples were then washed with HBS, and the cells of five independent observation fields were observed and counted on the whole sample thickness using a bright-field microscope with ×20 objective (Leica DM5500). Cell viability (in%) resulted from the ratio between the number of non-stained cells and the total cell number.

Finite Element Simulation: Finite element modeling (FEM) was performed in COMSOL version 4.3b. The gel and the cells were modeled as nearly incompressible linear elastic materials, while the pore space was considered void. The boundary conditions were set to free movement for all boundaries except for the top and bottom boundary, which were used to impose the compression in *z* direction. The simulations were run in 2D, using the SolidMechanics physics, with

DOI: 10.1002/adhm.201400250

an in-plane stress 2D approximation. The materials were all supposed to be linearly elastic with appropriate local Young moduli, and a Poisson ratio of 0.48.

Statistical Analysis: Unpaired, two-sided *t*-tests were used for direct comparison of pairs of outcome variables. To test whether the injection procedure had a significant effect on cell viability or neurite length, the difference between the outcome measures before and at a given time point after injection was compared to the difference at identical time points under control conditions by means of an adapted *t*-test with a compound estimation of the standard deviation and a corresponding adjustment of the number of degrees of freedom. To assess the relation between the initial polymer concentration and the local Young modulus, F-tests were applied to the analysis of variance associated with the linear regression. No multiple testing corrections were used. Error bars indicate standard deviations, except where otherwise noted.

Supporting Information

Supporting Information is available from the Wiley Online Library or from the author.

Acknowledgements

A.B. and T.B. contributed equally to this work. The authors thank the EPFL biomaging and optics core facilities, as well as the EPFL Molecular and Hybrid Materials Characterization Center, for their excellent technical assistance, and Blake Erickson for his help with the AFM imaging. This work was funded by the Swiss National Science Foundation, Grant PBELP3-133350, IZK0Z2_154342 and 205321_134786, by the Brazilian Swiss Joint Research Programme No.BJRP 0112-09 and by the European Research Council under the European Union's Seventh Framework Programme (FP7/2007-2013)/ERC grant agreement n°307338.

Received: May 13, 2014
Revised: July 31, 2014
Published online:

[1] T. Back, *Cell Mol. Neurobiol.* **1998**, *18*, 621.
[2] B. A. Reynolds, S. Weiss, *Science* **1992**, *255*, 1707.
[3] F. H. Gage, *Science* **2000**, *287*, 1433.
[4] K. van Kuyck, M. Welkenhuysen, L. Arckens, R. Sciot, B. Nuttin, *Neuromodulation* **2007**, *10*, 244.
[5] E. Bible, D. Y. S. Chau, M. R. Alexander, J. Price, K. M. Shakesheff, M. Modo, *Biomaterials* **2009**, *30*, 2985.
[6] D. Fon, A. Al-Abboodi, P. P. Chan, K. Zhou, P. Crack, D. I. Finkelstein, J. S. Forsythe, *Adv. Healthcare Mater.* **2014**, *3*, 761.
[7] C. R. Freed, P. E. Greene, R. E. Breeze, W. Y. Tsai, W. DuMouchel, R. Kao, S. Dillon, H. Winfield, S. Culver, J. Q. Trojanowski, D. Eidelberg, S. Fahn, *N. Engl. J. Med.* **2001**, *344*, 710.
[8] A. J. Mothe, T. Zahir, C. Santaguida, D. Cook, C. H. Tator, *PLoS One* **2011**, *6*, e27079.
[9] O. Lindvall, P. Brundin, H. Widner, S. Rehncrona, B. Gustavii, R. Frackowiak, K. L. Leenders, G. Sawle, J. C. Rothwell, C. D. Marsden, A. Björklund, *Science* **1990**, *247*, 574.
[10] M. Abematsu, K. Tsujimura, M. Yamano, M. Saito, K. Kohno, J. Kohyama, M. Namihira, S. Komiya, K. Nakashima, *J. Clin. Invest.* **2010**, *120*, 3255.
[11] S. Kriks, J. W. Shim, J. Piao, Y. M. Ganat, D. R. Wakeman, Z. Xie, L. Carrillo-Reid, G. Auyeung, C. Antonacci, A. Buch, L. Yang, M. F. Beal, D. J. Surmeier, J. H. Kordower, V. Tabar, L. Studer, *Nature* **2011**, *480*, 547.
[12] T. Yuan, W. Liao, N. H. Feng, Y. L. Lou, X. Niu, A. J. Zhang, Y. Wang, Z. F. Deng, *Stem Cell Res. Ther.* **2013**, *4*, 73.
[13] R. M. Richardson, A. Singh, D. Sun, H. L. Fillmore, D. W. Dietrich, M. R. Bullock, *J. Neurosurg.* **2010**, *112*, 1125.
[14] A. Farin, C. Y. Liu, I. A. Langmoen, M. L. J. Apuzzo, *Neurosurgery* **2009**, *65*, 831.
[15] T. C. Burns, G. K. Steinberg, *Expert Opin. Biol. Ther.* **2011**, *11*, 447.
[16] P. Moshayedi, G. Ng, J. C. Kwok, G. S. Yeo, C. E. Bryant, J. W. Fawcett, K. Franze, J. Guck, *Biomaterials* **2014**, *35*, 3919.
[17] S. Zhou, A. Bismarck, J. H. G. Steinke, *J. Mater. Chem. B* **2013**, *1*, 4736.
[18] A. J. Thornton, E. Alsberg, M. Albertelli, D. J. Mooney, *Transplantation* **2004**, *77*, 1798.
[19] S. A. Bencherif, R. W. Sands, D. Bhatta, P. Arany, C. S. Verbeke, D. A. Edwards, D. J. Mooney, *Proc. Natl. Acad. Sci. U.S.A.* **2012**, *109*, 19590.
[20] V. I. Lozinsky, I. Y. Galaev, F. M. Plieva, I. N. Savina, H. Jungvid, B. Mattiasson, *Trends Biotechnol.* **2003**, *21*, 445.
[21] M. Jurga, M. B. Dainiak, A. Sarnowska, A. Jablonska, A. Tripathi, F. M. Plieva, I. N. Savina, L. Strojek, H. Jungvid, A. Kumar, B. Lukomska, K. Domanska-Janik, N. Forraz, C. P. McGuckin, *Biomaterials* **2011**, *32*, 3423.
[22] H. Yang, W. O'Hali, H. Kearns, J. R. Wright Jr, *Transplantation* **1997**, *64*, 28.
[23] T. Miyamoto, S. Takahashi, H. Ito, H. Inagaki, Y. Noishiki, *J. Biomed. Mater. Res.* **1989**, *23*, 125.
[24] M. Matyash, F. Despang, R. Mandal, D. Fiore, M. Gelinsky, C. Ikonomidou, *Tissue Eng. Part A* **2012**, *18*, 55.
[25] T. Koike, S. E. Pfeiffer, *Dev. Neurosci.* **1979**, *2*, 177.
[26] J. H. Lee, J. P. Singer, E. L. Thomas, *Adv. Mater.* **2012**, *24*, 4782.
[27] P. B. Welzel, J. Friedrichs, M. Grimmer, S. Vogler, U. Freudenberg, C. Werner, *Adv. Healthcare Mater.* **2014**, DOI:10.1002/adhm.201400102.
[28] L. J. Gibson, M. F. Ashby, *Cellular Solids: Structure and Properties*, Cambridge University Press, Cambridge, UK **1997**.
[29] H. Metz, J. McElhaney, A. K. Ommaya, *J. Biomech.* **1970**, *3*, 453.
[30] Z. Taylor, K. Miller, *J. Biomech.* **2004**, *37*, 1263.
[31] G. T. Fallenstein, V. D. Hulce, J. W. Melvin, *J. Biomech.* **1969**, *2*, 217.
[32] H. Kirsebom, G. Rata, D. Topgaard, B. Mattiasson, I. Y. Galaev, *Macromolecules* **2009**, *42*, 5208.
[33] E. Spedden, J. D. White, E. N. Naumova, D. L. Kaplan, C. Staii, *Biophys. J.* **2012**, *103*, 868.
[34] R. C. Weast, M. J. Astle, W. H. Beyer, *Handbook of Chemistry and Physics*, 64th ed., CRC Press, Inc., Boca Raton, FL, USA **1984**.
[35] H. Czichos, *Hütte: Die Grundlagen der Ingenieurwissenschaften*, Springer Verlag, Berlin **2000**.
[36] B. M. A. Carvalho, S. L. Da Silva, L. H. M. Da Silva, V. P. R. Minim, M. C. H. Da Silva, M. L. Carvalho, L. A. Minim, *Separation Purification Rev.* **2014**, *43*, 241.
[37] E. Garbayo, G. Delcroix, P. C. Schiller, C. N. Montero-Menei, in *Tissue Engineering of Tissue and Organ Regeneration*, (Ed: D. Eberli), Intech, Rijeka, Croatia **2011**.
[38] P. Brundin, G. Barbin, O. Isacson, M. Mallat, B. Chamak, A. Prochiantz, F. H. Gage, A. Bjorklund, *Neurosci. Lett.* **1985**, *61*, 79.
[39] R. N. Nye, T. B. Mallory, *Boston Med. Surg. J.* **1923**, *189*, 561.
[40] Y. Sun, Z. Huang, W. Liu, K. Yang, K. Sun, S. Xing, D. Wang, W. Zhang, X. Jiang, *Biointerphases* **2012**, *7*, 29.
[41] R. Lanza, R. Langer, J. Vacanti, *Principles of Tissue Engineering*, Academic Press, London **2013**.

[42] A. Tripathi, N. Kathuria, A. Kumar, *J. Biomed. Mater. Res. A* **2009**, *90*, 680.
[43] A. Schuz, G. Palm, *J. Comp. Neurol.* **1989**, *286*, 442.
[44] M. C. Laplaca, V. N. Vernekar, J. T. Shoemaker, D. K. Cullen, in *Methods in Bioengineering: 3D Tissue Engineering*, (Eds: F. Berthiaume, J. Morgan), Artech House Publishers, London **2010**.
[45] B. Nadarajah, P. Alifragis, R. O. Wong, J. G. Parnavelas, *Nat. Neurosci.* **2002**, *5*, 218.
[46] H. Kaji, G. Camci-Unal, R. Langer, A. Khademhosseini, *Biochim. Biophys. Acta* **2011**, *1810*, 239.
[47] A. Beduer, I. Gonzales-Calvo, C. Vieu, I. Loubinoux, L. Vaysse, *Macromol. Biosci.* **2013**, *13*, 1546.
[48] S. M. Frisch, E. Ruoslahti, *Curr. Opin. Cell Biol.* **1997**, *9*, 701.
[49] M. L. Previtera, C. G. Langhammer, B. L. Firestein, *J. Biosci. Bioeng.* **2011**, *110*, 459.
[50] X. Zhao, N. Huebsch, D. J. Mooney, Z. Suo, *J. Appl. Phys.* **2010**, *107*, 63509.
[51] T. Braschler, A. Valero, L. Colella, K. Pataky, J. Brugger, P. Renaud, *Lab Chip* **2010**, *10*, 2771.

Adv. Healthcare Mater. **2014**,
DOI: 10.1002/adhm.201400250